

■ Organic–Inorganic Hybrid Composites | *Hot Paper* |

Luminescent PMMA Films and PMMA@SiO₂ Nanoparticles with Embedded Ln³⁺ Complexes for Highly Sensitive Optical Thermometers in the Physiological Temperature Range**

 Dimitrije Mara,^{*[a, b]} Anna M. Kaczmarek,^{*[a]} Flavia Artizzu,^[a] Anatolii Abalymov,^[c, d] Andre G. Skirtach,^[c] Kristof Van Hecke,^[a] and Rik Van Deun^[a]

Abstract: In recent years, luminescent materials doped with Ln³⁺ ions have attracted much attention for their application as optical thermometers based on both downshifting and upconversion processes. This study presents research done on the development of highly sensitive optical thermometers in the physiological temperature range based on poly(methyl methacrylate) (PMMA) films doped with two series of visible Ln³⁺ complexes (Ln³⁺ = Tb³⁺, Eu³⁺, and Sm³⁺) and SiO₂ nanoparticles (NPs) coated with these PMMA films. The best performing PMMA film doped with Tb³⁺ and Eu³⁺ complexes was the PMMA[TbEuL₁tppo]1 film (L₁ = 4,4,4-trifluoro-1-phenyl-1,3-butadionate; tppo = triphenylphosphine oxide), which showed good temperature sensing of S_r = 4.21 % K⁻¹

at 313 K, whereas for the PMMA films doped with Tb³⁺ and Sm³⁺ complexes the best performing was the PMMA[TbSmL₂tppo]3 film (L₂ = 4,4,4-trifluoro-1-(4-chlorophenyl)-1,3-butadionate), with S_r = 3.64 % K⁻¹ at 313 K. Additionally, SiO₂ NPs coated with the best performing films from each of the series of PMMA films (Tb–Eu and Tb–Sm) and their temperature-sensing properties were studied in water, showing excellent performance in the physiological temperature range (PMMA[TbEuL₁tppo]1@SiO₂: S_r = 3.84 % °C at 20 °C; PMMA[TbSmL₂tppo]3@SiO₂: S_r = 3.27 % °C at 20 °C) and the toxicity of these nanoparticles on human cells was studied, showing that they were nontoxic.

Introduction

Temperature is one of the fundamental thermodynamic properties that can influence physical, chemical, or biological processes.^[1] The accurate and precise measurement of temperature is needed for different industrial and technological developments and scientific research, such as aerospace, automo-

otive, metrology, electronics, cell biology, nanomedicine, and biomedicine.^[2–10] In biotechnological applications and biological research, the reactivity and dynamics of the biomolecules are correlated with temperature. Elevated temperature in an organism can indicate that there is a physiological disorder, such as illness.^[7] For example, cancer cells show a higher temperature than that of normal cells. The reason for this difference in temperature is the higher metabolism of cancer cells.^[11,12] One of the ways to measure temperature in cells is to employ luminescent thermometry measurements because they are noncontact, give a real-time response, and have precision at the molecular level.^[13]

Organic dyes have been extensively used for this purpose, yet they show certain drawbacks, such as short excited-state lifetimes, small Stokes shifts, broad emission bands, photobleaching, and their emission intensity depends on the local environment.^[7,14–18] Alternatively, lanthanide (Ln³⁺) ions have large Stokes shifts, narrow and sharp emission bands, long excited-state lifetimes, and their luminescence properties are less dependent on the local environment, and therefore, they are very attractive for luminescent sensing applications.^[19–23] Lanthanide emission is based on the parity-forbidden 4f – 4f transitions, and direct excitation of Ln³⁺ is therefore an inefficient process because of the low molar extinction coefficients. To avoid this limitation, Ln³⁺ can form complexes with organic ligands, in which these ligands can act as sensitizers to increase the absorption of light and transfer the absorbed energy to

[a] Dr. D. Mara, Prof. A. M. Kaczmarek, Dr. F. Artizzu, Prof. K. Van Hecke, Prof. R. Van Deun
Department of Chemistry, Ghent University
Krijgslaan 281-53, 9000 Ghent (Belgium)
E-mail: anna.kaczmarek@ugent.be

[b] Dr. D. Mara
Department of Chemistry, KU Leuven
Celestijnenlaan 200D, 3001 Leuven (Belgium)
E-mail: dimitrije.mara@kuleuven.be

[c] A. Abalymov, Prof. A. G. Skirtach
Department of Biotechnology, Ghent University
Coupure Links 653, 9000 Ghent (Belgium)

[d] A. Abalymov
Educational Research Institute of Nanostructure and Biosystems
Saratov State University, Saratov 410012 (Russia)

[**] PMMA = poly(methyl methacrylate).

 Supporting information and the ORCID identification number(s) for the author(s) of this article can be found under:
<https://doi.org/10.1002/chem.202004951>. It contains details on the synthesis of lanthanide β-diketonate complexes; crystal data and refinement details; FTIR, ESI-MS, and TGA-DTA data; a discussion on the photoluminescence properties; and a discussion on temperature-dependent samples.

the lanthanide ions. Organic molecules, which can be employed as sensitizers, are, for example, heterocyclic, aromatic carboxylates or β -diketonates as ligands.^[24–26] The long excited-state lifetimes of lanthanide probes versus the short excited-state lifetimes of organic dyes present a clear advantage in biological experiments: the fluorescence of a typical organic molecule will be observable for about the same amount of time as that of the autofluorescence of biomolecules, whereas the emitted light of a Ln^{3+} probe is longer lived. Therefore, if Ln^{3+} probes can be made to bind selectively to certain parts of tumor cells, these can be very precisely located by using the longer-lived lanthanide luminescence.

Lanthanide molecular structures based on β -diketonate complexes retain high color purity and quantum yields. β -Diketonate ligands possess high energetic singlet and triplet levels, which makes them suitable for exciting Ln^{3+} . Furthermore, they have a strong affinity to form stable complexes with Ln^{3+} because they are hard Lewis bases and Ln^{3+} are hard Lewis acids. With Ln^{3+} , they mostly form tris complexes, leaving two vacant coordination sites, which can be occupied by water molecules or by additional neutral ligands. This creates the opportunity to change the chemical properties just by changing the coordination environment. Furthermore, these compounds can be easily processed into complex matrices, such as organic polymers, silica glasses, or other materials.^[27]

Herein, we report on the synthesis, photoluminescence (PL), and sensing properties of poly(methyl methacrylate) (PMMA) films and SiO_2 nanoparticles (NPs) coated with PMMA films doped with luminescent tris- β -diketonate lanthanide complexes (Figure 1). The lanthanide β -diketonate complexes with L_1 or L_2 ligands were isolated as water-free molecules in which the neutral tppo molecules completed the coordination sphere. The complexes of Eu^{3+} and Tb^{3+} are new complexes reported herein, whereas the complexes of Sm^{3+} were reported in our previous study.^[28] The best performing complexes, selected on the basis of their photoluminescent properties and emission quantum yields, were incorporated as dopants in transparent and flexible PMMA films.^[29] PMMA was chosen as a homogenous material, in which two different complexes could

be doped to obtain ratiometric thermometers. In particular, doping was carried out with two systems consisting of $\text{Tb}^{3+} - \text{Eu}^{3+}$ and $\text{Tb}^{3+} - \text{Sm}^{3+}$ mixed-metal complexes, which were already proved to show promising temperature-sensing properties in the physiological range.^[30] Although the $\text{Tb}^{3+} - \text{Eu}^{3+}$ system is an already popular thermometer in the physiological temperature range,^[5,13,31–34] the $\text{Tb}^{3+} - \text{Sm}^{3+}$ system is rarely investigated, despite its promising potential, due to the difficulty in obtaining an intense Sm^{3+} emission at temperatures above room temperature.^[35,36] Finally, to explore the potential of these materials to be used as thermometers in biological applications, SiO_2 NPs coated with doped PMMA films were investigated.

Results and Discussion

Preparation and optimization of doped PMMA films

The optimized synthesis of the doped PMMA films is described in the Experimental Section. The polymerization of PMMA and the conditions for doping the lanthanide complexes into the polymer were first optimized. In the first attempts, different solvents were used to dissolve PMMA (acetonitrile and methanol, pure acetonitrile, dichloromethane, and chloroform). Chloroform was identified as the best solvent to codissolve PMMA and the complexes. The second step of optimizing the film preparation was finding the optimal ratio between the two complexes $[\text{Ln}_1(\text{L}_{1(2)})_3(\text{tppo})_2]$ and $[\text{Ln}_2(\text{L}_{1(2)})_3(\text{tppo})_2]$ ($\text{Ln}_1 = \text{Tb}^{3+}$; $\text{Ln}_2 = \text{Eu}^{3+}$ or Sm^{3+}), which would give the desired luminescent properties (see the PL studies of complexes in the Supporting Information) and would allow the final materials to be used for temperature-sensing properties. Table 1 gives the optimized ratios of Ln_1 to Ln_2 complexes in PMMA films. The films were obtained by slow solvent evaporation at 30°C in Petri dishes with a diameter of 70 mm. Transparent films with Ln^{3+} complexes were obtained (Figure 2). PL characterization was carried out before the samples were investigated for tem-

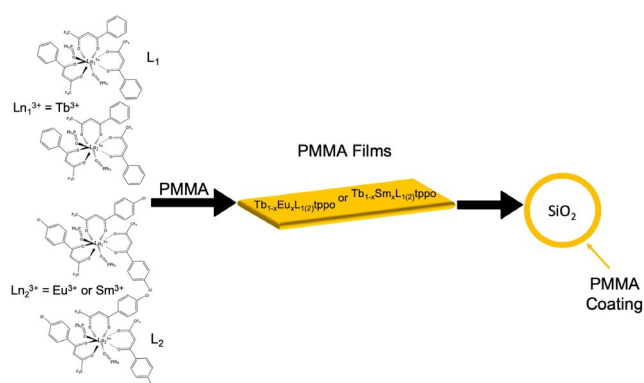


Figure 1. Schematic representation of the approach employed herein. From the free complex to PMMA-coated SiO_2 NPs; $\text{L}_1 = 4,4,4$ -trifluoro-1-phenyl-1,3-butadione, $\text{L}_2 = 4,4,4$ -trifluoro-1-(4-chlorophenyl)-1,3-butadione; tppo = tri-phenylphosphine oxide.

Table 1. Molar ratio of doped lanthanide complexes ($\text{Ln}_1 = \text{Tb}^{3+}$; $\text{Ln}_2 = \text{Eu}^{3+}$, Sm^{3+}) after optimization in PMMA films, with general formulas of LnL_1tppo and LnL_2tppo .

Sample ^[a]	Ln_1	Ln_2
PMMA[TbEuL ₁ tppo]1	12	1
PMMA[TbEuL ₁ tppo]2	16	1
PMMA[TbEuL ₁ tppo]3	20	1
PMMA[TbEuL ₂ tppo]1	30	1
PMMA[TbEuL ₂ tppo]2	34	1
PMMA[TbEuL ₂ tppo]3	38	1
PMMA[TbSmL ₁ tppo]1	4	1
PMMA[TbSmL ₁ tppo]2	6	1
PMMA[TbSmL ₁ tppo]3	10	1
PMMA[TbSmL ₂ tppo]1	4	1
PMMA[TbSmL ₂ tppo]2	12	1
PMMA[TbSmL ₂ tppo]3	16	1

[a] The numbers 1–3 in labels represent the different doping ratios of the Ln_1 and Ln_2 in PMMA films presented in this table. Each number corresponds to an individual ratio from this table.

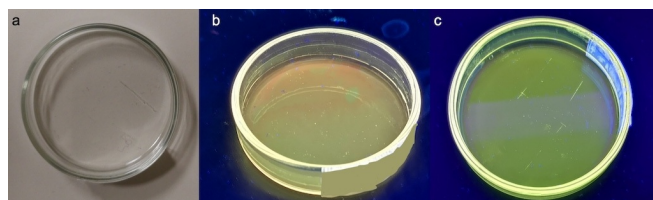


Figure 2. Photographs of PMMA Ln³⁺-doped films: a) the transparent PMMA[Ln₁Ln₂L₁₍₂₎tppo] film, b) PMMA[TbEuL₁tppo]1 under a UV lamp with excitation at 365 nm, and c) PMMA[TbSmL₂tppo]3 under a UV lamp with excitation at 365 nm.

perature-dependent luminescence sensing. A brief discussion of the results obtained for the PL properties of the PMMA films is given with Figures S32–S35 and Tables S3 and S4 in the Supporting Information.

PMMA-coated SiO₂ NPs

Two different methods of coating the SiO₂ NPs were investigated. As a model complex, EuL₁tppo-doped PMMA was used. The first method was based on the sonication of a suspension of SiO₂ NPs with PMMA for 30 min. The second method consisted of vigorous stirring of a suspension of SiO₂ NPs with PMMA for 30 min; in both methods, chloroform was used as the solvent. After sonication or stirring, the SiO₂ NPs were separated from the solution by centrifugation and left for 1 d to dry in air. Next, the NPs were washed once with a mixture of methanol and water to remove all residuals of the synthesis. The luminescent properties of coated SiO₂ NPs were then studied, and the intensity of the emitted light provided an indication of the homogeneity and thickness of the coating layer. Results for the PMMA@SiO₂ NPs samples showed that the second method was more efficient in coating of the silica NPs. The stirring process was further prolonged to 2 h to ensure complete coating of the SiO₂ NPs. SEM and TEM images of the PMMA@SiO₂ NPs are shown in Figure 3. After the coating process, there were no visible changes in the size and shape of the particles, ranging from 150 to 500 nm in diameter (Figures S19–S22 in the Supporting Information). Upon higher magnification, a thin coating with a thickness of about 7 nm can be observed on the particle surface (see Figure 3 d).

Luminescent thermometry

Luminescent thermometers can be based on different principles, such as the measurement of luminescence lifetimes, shifts of the emission peaks, or changes to the luminescence intensity of one or more emission peaks.^[2,37] In this case, luminescent thermometry based on emission intensity was chosen. There are two types of ratiometric emission intensity thermometry methods. The difference is based on the number of emission centers present in the materials. Single-center ratiometric-based luminescent thermometers are based on a single emission center, in which both emission peaks are generated from two different excited levels, which are in thermal equilibrium of the same emitting center. Because these levels are thermally

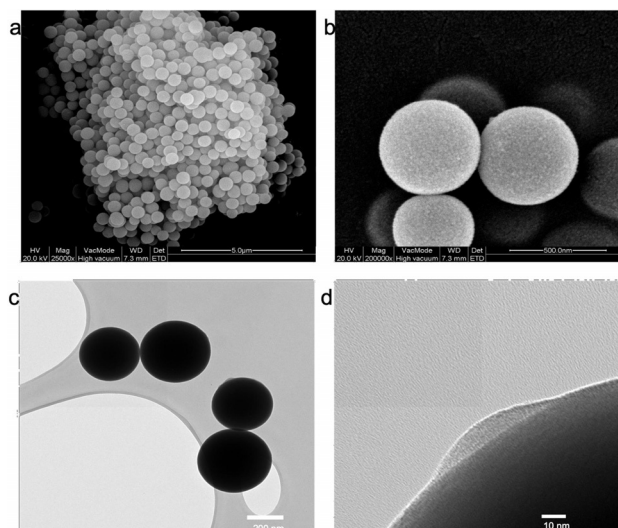


Figure 3. SEM and TEM images of SiO₂ NPs coated with a PMMA-[TbEuL₁tppo]1 film: a) dispersion of the particles, b) magnification of the SiO₂ NPs by SEM, c) particles, and d) magnification of the surface of SiO₂ NPs showing PMMA coating by TEM.

coupled for these type of thermometers, external thermal calibration of the thermometric parameter is needed. The calibration process requires an independent measurement by using, for example, a thermocouple or infrared camera, which allows the intensity-to-temperature conversion. The dual-center-based luminescent thermometers overcome these disadvantages by possessing two emitting centers. In this type of thermometer, the emitting center can be thermally coupled, but, in most cases, they are not, and thus, external calibration of the thermometric parameter is not necessary.^[22] Herein, the ion pairs of Tb³⁺ – Eu³⁺ and Tb³⁺ – Sm³⁺ as systems for dual-center ratiometric thermometers were chosen. To calculate the thermometric parameter Δ , Equations (1) and (2) were used:^[38]

$$\Delta = \frac{I_1}{I_2} \quad (1)$$

$$\Delta = \frac{\Delta_0}{1 + \alpha \exp\left(-\frac{\Delta E}{k_B T}\right)} \quad (2)$$

in which I_1 (Tb³⁺ = ⁵D₄ → ⁷F₅) and I_2 (Eu³⁺ = ⁵D₀ → ⁷F₂ or Sm³⁺ = ⁵G_{5/2} → ⁶H_{9/2}) are integrated intensities of the transitions, Δ_0 is Δ ($T = 0$ K), α presents the ratio between nonradiative (W_0 at $T = 0$ K) and radiative (W_r) rates, and ΔE is the activation energy for the nonradiative pathway. The S_r value indicates the relative change of the thermometric parameter per degree of the temperature change (%K⁻¹) and was calculated by using Equation (3):

$$S_r = 100\% \left[\frac{1}{\Delta} \frac{\partial \Delta}{\partial T} \right] \quad (3)$$

which is inversely proportional to the thermometric parameter (Δ) and the variation of the thermometric parameter ($\partial \Delta$) per temperature variation (∂T). The S_r value is used for a compari-

son of thermometers composed of different materials and it is independent of the nature of the thermometer. The maximal value of the relative sensitivity for the measured temperature range can be presented as S_m .

The performance and stability of the thermometer is estimated by cycling the temperature in the given temperature interval, ensuring that the thermometer reaches thermal equilibrium for each measurement. It can be described by Equation (4):

$$R = 1 - \frac{\max(|\Delta_c - \Delta_i|)}{\Delta_c} \quad (4)$$

in which Δ_c is the mean thermometric parameter extracted from the calibration curve, and Δ_i is the value of each thermometric parameter measurement.^[22]

The temperature uncertainty, δT , is an important parameter in the assessment of the performance of the desired thermometer. δT can be calculated by using Equation (5):

$$\delta T = \frac{1}{S_r} \frac{\delta \Delta}{\Delta} \quad (5)$$

Temperature-dependent luminescence of

PMMA[Ln₁Ln₂L₁₍₂₎tppo] films (Ln₁ = Tb³⁺; Ln₂ = Eu³⁺ or Sm³⁺)

The temperature-dependent luminescence was measured in the physiological temperature region, which was extended down to 253 K (−20 °C) for the samples of this series because of interest from fundamental studies of the biological, biochemical, and physiological processes occurring in cells if they have been frozen. During defrosting, there is the need to accurately measure the temperature, while these physiological processes are monitored.

For the PMMA[TbEuL₁₍₂₎tppo] films, six samples were studied for their temperature-dependent luminescence properties: three with L₁ and three with L₂ ligands. Of these, the PMMA-[TbEuL₁tppo]1 sample is discussed in detail, whereas the other two samples are discussed in detail in the Supporting Information (Figures S36 and S37).

The integrated areas under the peaks used for these samples are, for Tb³⁺, the ⁵D₄→⁷F₅ transition peak, which is observed between 533 and 558 nm, and for Eu³⁺, the ⁵D₀→⁷F₂ transition peak, which is observed between 604 and 630 nm.

An emission map of PMMA[TbEuL₁tppo]1, which is measured in the temperature range from 253 to 353 K, is presented in Figure 4a. The I_{543}/I_{614} intensity ratio of the integrated areas under the peaks for PMMA[TbEuL₁tppo]1 was calculated (Figure 4b), for the indicated temperature range, over which the sample showed monotonic behavior. The data points were fitted with Equation (2), yielding $\Delta E = 3537 \text{ cm}^{-1}$ ($R^2 = 0.9993$). The calculated energy difference between the emitting level of Tb³⁺ (⁵D₄ = 20 500 cm^{−1}) and the emitting level of Eu³⁺ (⁵D₀ = 17 300 cm^{−1}), which is $\Delta E = 3200 \text{ cm}^{-1}$. In Figure 4c, the relative sensitivity, S_r , is presented at different temperatures. The maximum value of $S_r = 4.21 \% \text{ K}^{-1}$ obtained at 313 K indicates

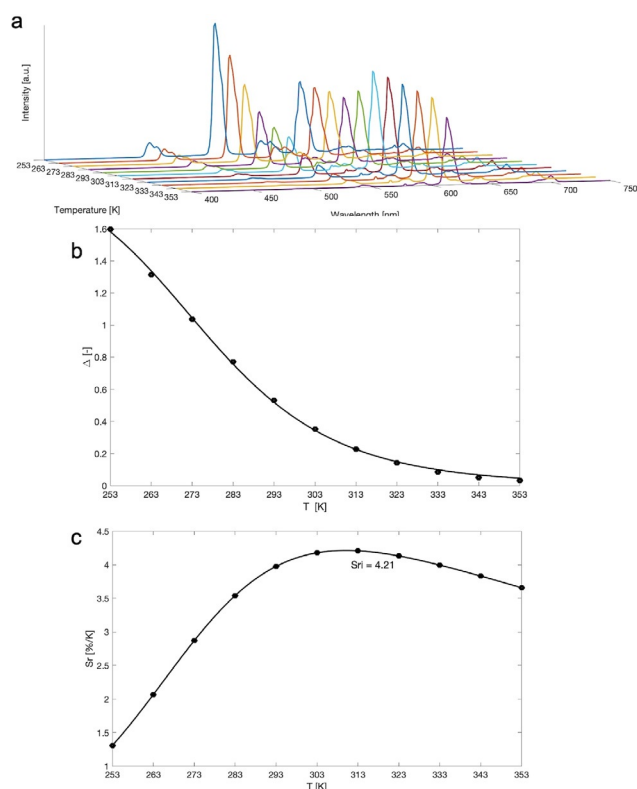


Figure 4. a) Emission map of the PMMA[TbEuL₁tppo]1 film, as measured over the 253–353 K range (step 10 K). b) Plot representing the calibration curve for PMMA[TbEuL₁tppo]1. The points show the experimental Δ parameter and the solid line is the best fit of the experimental points obtained from Equation (2). c) Plot showing the relative sensitivity, S_r values at different temperatures (253–353 K); the solid line is intended as a guide.

that this sample has one of the highest S_r values over the physiological temperature range reported, to date (Table 2).

For the films from the PMMA[TbEuL₂tppo] series, the best results were obtained for the PMMA[TbEuL₂tppo]3 sample. A detailed discussion of the temperature-dependent luminescence of this sample and the other two samples in the series is presented in the Supporting Information. For the PMMA-[TbEuL₂tppo]3 sample, the maximal value of the relative sensitivity, $S_r = 4.04 \% \text{ K}^{-1}$, was obtained at 313 K.

Similarly, six PMMA[TbSmL₁₍₂₎tppo] films were investigated for their temperature-dependent luminescence properties and ability to work as temperature sensors. For both ligands L₁ and L₂, three samples were investigated.

The integrated peaks used for these samples were at 543 nm (⁵D₄→⁷F₅) for the Tb³⁺ ion, which was integrated over the range between 533 and 558 nm, and the Sm³⁺ ion peak at 643 nm (⁵G_{5/2}→⁶H_{9/2}), which was integrated over the range of 630–660 nm.

For the samples from the PMMA[TbSmL₁tppo] series, of the three investigated samples, the best results were obtained for PMMA[TbSmL₁tppo]1, which is discussed in detail, along with the other two samples, in the Supporting Information. For the PMMA[TbSmL₁tppo]1 sample, a maximal relative sensitivity of $S_r = 3.45 \% \text{ K}^{-1}$ was obtained at 313 K.

In the series of the samples with general formula PMMA[TbSm₂tppo], the sample showing the best results is PMMA[TbSm₂tppo]3 and is discussed herein, whereas the other two samples are discussed in the Supporting Information (Figures S44 and S45).

An emission map of the PMMA[TbSm₂tppo]3 sample, which is measured over the temperature range from 253 to 343 K, is presented in Figure 5a. The I_{543}/I_{643} intensity ratio of the integrated areas under the peaks for PMMA[TbSm₂tppo]3 was calculated (Figure 5b) for the indicated temperature range and showed monotonic behavior. Fitting of the data points was performed by using Equation (2), yielding $\Delta E = 3274 \text{ cm}^{-1}$ ($R^2 = 0.9994$). The calculated energy difference can be best matched by the energy difference between the triplet level ($T_1 = 24000 \text{ cm}^{-1}$) of the tppo ligand and the emitting level of Tb³⁺ ($^5D_4 = 20500 \text{ cm}^{-1}$), which is $\Delta E = 3500 \text{ cm}^{-1}$. In Figure 5c, the relative sensitivity, S_r , is presented, as calculated for different temperatures. The maximum value of $S_r = 3.64\% \text{ K}^{-1}$ obtained at 313 K indicates that this sample is a very good temperature point in the physiological range. In Table 2, a comparison of the materials reported herein with known materials from literature is presented.

The results for the Tb³⁺ – Eu³⁺ materials from this study have shown very good relative sensitivities compared with those of other Tb³⁺ – Eu³⁺ materials reported in the literature (Table 2). They are much more sensitive, even up to seven

times. Although the results for samples based on the Tb³⁺ – Sm³⁺ system show that their relative sensitivity is slightly higher than those of similar systems with only one material,^[36] it has nevertheless shown higher sensitivity. A comparison of our samples with different systems, such as hybrid systems or organic dyes, shows similar or higher sensitivity, even up to four times.

To show the potential of the thermometer materials for real applications, stability tests were carried out, in which the samples were subjected to three heating/cooling cycles. The stability tests for the PMMA[TbEu₂tppo]3 and PMMA[TbSm₁tppo]1 samples are presented in Figure 6, showing a repeatability of up to 95% for PMMA[TbEu₂tppo]3 and up to 97% for PMMA[TbSm₁tppo]1. The temperature uncertainty for these two compounds has been calculated and it is presented in Supporting Information (Figure S46). The proposed energy-transfer (ET) mechanisms based on results obtained for samples from both systems are presented in Figure 7.

Temperature sensing of PMMA-coated SiO₂ NPs in water

For SiO₂ NPs coated with PMMA films containing lanthanide complexes, the temperature-sensing capability was studied in water over the 5 (278) to 50 °C (323 K) temperature range. It is known that water is an efficient quencher of the luminescence properties of the lanthanide ions through vibrational quench-

Table 2. A comparison of the sensitivity of the reported thermometers with the sensitivity of other luminescent thermometers over the physiological temperature range. An overview of the materials, temperature range [K], and maximal relative sensitivity values (S_m) is given.

Material ^[a]	T range [K]	S_m [% K ⁻¹] ([K])	Ref.
[Eu _{0.53} Tb _{0.47} (tfac) ₈]Na ₂	273–373	2.70 (353)	[30]
[Tb _{0.90} Sm _{0.10} (tfac) ₈]Na ₂	280–360	2.30 (360)	[30]
Eu _{0.56} Tb _{0.50} DPA-PMO	260–460	1.56 (360)	[35]
Sm _{0.95} Tb _{0.05} DPA-PMO	280–460	2.38 (340)	[35]
BPy-PMO@Tb,Sm(acac) ₃ _10_90	253–333	4.93 (253)	[36]
Tb _{0.92} Eu _{0.08} -HPIDC-OX	303–473	0.6 (473)	[39]
[Ln(ad) _{0.5} (phth)(H ₂ O) ₂] (Ln = 5Eu ^{III} /10Tb ^{III})	303–423	1.21 (303)	[40]
Tb@UiO-66 hybrid film	303–353	2.76 (303)	[41]
Eu@UiO-66 hybrid film	303–403	4.26 (363)	[41]
Ca _{8.98} Mg _{1.5} (PO ₄) ₇ :x(Eu ²⁺ , Eu ³⁺)	293–473	1.192 (383)	[42]
[Tb _{0.97} Eu _{0.03} (L)(OX)(H ₂ O)]	250–340	1.38 (340)	[43]
Eu _{0.05} -Tb _{1.95} -PDC	298–333	1.37 (333)	[44]
Tb _{0.8} Eu _{0.2} BPDA	293–328	1.19 (313)	[45]
(Tb/Eu-TPTZ)PMMA	298–373	2.98 (373)	[46]
ZJU-88J▷perylene	293–353	1.28 (293)	[47]
PMMA[TbEu ₁ tppo]1	253–353	4.21 (313)	this work
PMMA[TbEu ₁ tppo]2	253–353	3.99 (313)	this work
PMMA[TbEu ₁ tppo]3	253–353	3.81 (313)	this work
PMMA[TbEu ₂ tppo]1	253–343	3.57 (293)	this work
PMMA[TbEu ₂ tppo]2	253–343	3.78 (303)	this work
PMMA[TbEu ₂ tppo]3	253–343	4.04 (313)	this work
PMMA[TbSm ₁ tppo]1	253–373	3.45 (313)	this work
PMMA[TbSm ₁ tppo]2	253–353	3.15 (313)	this work
PMMA[TbSm ₁ tppo]3	253–343	2.93 (313)	this work
PMMA[TbSm ₂ tppo]1	253–373	3.39 (333)	this work
PMMA[TbSm ₂ tppo]2	253–333	3.50 (323)	this work
PMMA[TbSm ₂ tppo]3	253–343	3.64 (313)	this work

[a] tfac = 1,1,1-trifluoroacetylacetone, DPA = pyridine dicarboxamide, PMO = periodic mesoporous organosilica, BPy = 2,2'-bipyridyl, acac = acetylacetonate, H₃PIDC = 2-pyridin-4-yl-4,5-imidazoledicarboxylic acid, OX = oxalate, ad = adipate, phth = phthalate, PDC = pyridine-2,6-dicarboxylate, H₂BPDA = 1,1'-biphenyl-3,3'-dicarboxylic acid, TPTZ = 2,4,6-tris(2-pyridyl)-1,3,5-triazine.

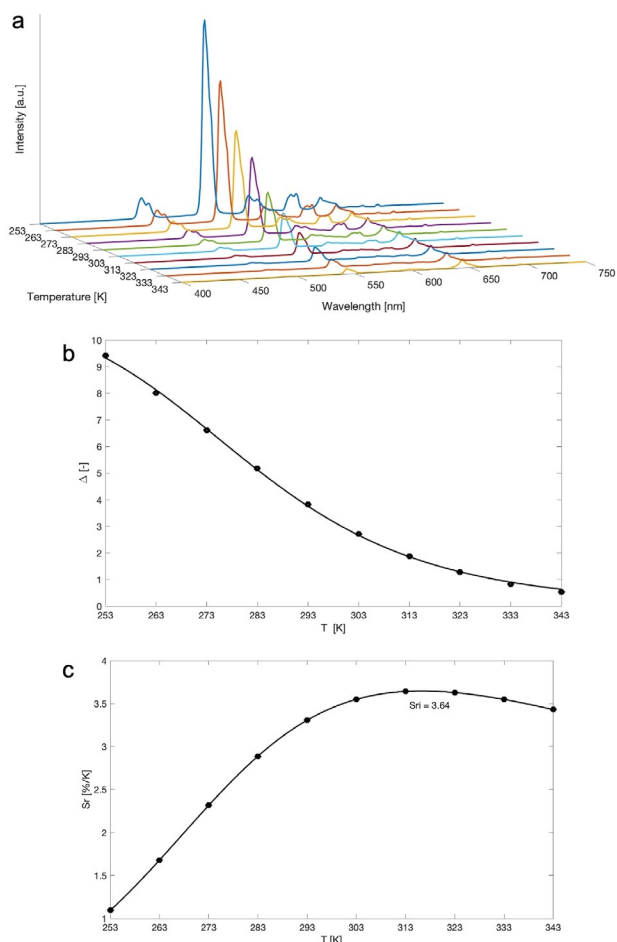


Figure 5. a) Emission map of the PMMA[TbSmL₂,ttpo]3 film, measured over the 253–343 K range (step 10 K). b) Plot representing the calibration curve for PMMA[TbSmL₂,ttpo]3. The points show the experimental Δ parameter and the solid line is the best fit of experimental points from Equation (2). c) Plot showing the relative sensitivity, S_r , values at different temperatures (253–343 K); the solid line is intended as a guide to the eye.

ing.^[27] For this reason, it is taken as a case study for these preliminary measurements. Cells and the whole human body consist of up to 70% water. However, the cytosol, in addition to water, also contains salts, proteins, and other biomolecules, which were not taken into consideration at this point of study. This and in vitro temperature-sensing studies will be a part of future investigations. As four coated PMMA films, two samples with the best performing temperature-sensing properties from the Tb³⁺ – Eu³⁺ system and two from the Tb³⁺ – Sm³⁺ system and one of each from both systems were taken from the series of the films, which consisted of sample derivatives with L₁ and L₂ complexes. The integrated areas of the peaks, which were used for calculations in both systems, are given in the last section. The stability of the PMMA-coated SiO₂ NPs was investigated after having been dispersed in water for one month. It was observed that the emission intensity of the Ln³⁺ complexes embedded in the PMMA film was reduced by about 20% relative to the initial measurements. A decrease in the emission intensity could be due to partial diffusion of water molecules in the PMMA polymer, which can then partially quench the Ln³⁺ emission.

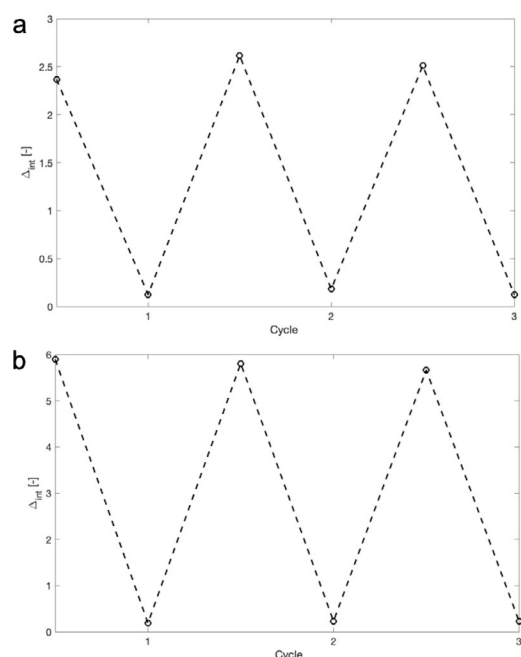


Figure 6. Temperature cycling tests for PMMA[TbEuL₂,ttpo]3 (a) and PMMA[TbSmL₁,ttpo]1 (b) over the temperature range of 253 to 373 K. The dashed lines are intended as a visual guide to the eye.

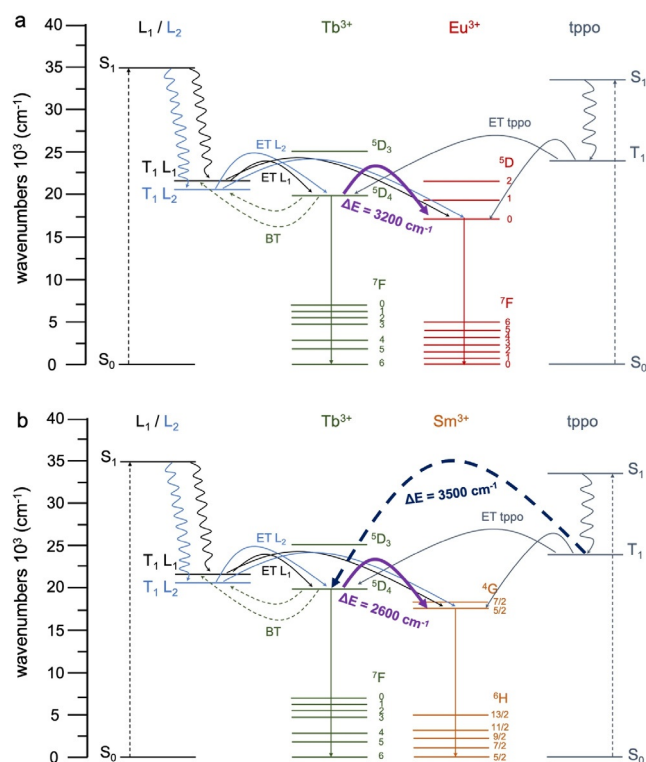


Figure 7. Energy-level diagram presenting the mechanism of ET in a) PMMA[TbEuL₂,ttpo] films and PMMA[TbEuL₂,ttpo]@SiO₂ NPs, and b) PMMA[TbSmL₁,ttpo] films and PMMA[TbSmL₁,ttpo]@SiO₂ NPs. S₀ and S₁ are the singlet ground level and singlet excited level, respectively; T₁ is the triplet level; ET is to the lanthanide ions from the ligands; BT is the energy back transfer; ΔE represents the energy gap and is indicated in a) in purple for both series of samples and in b) in purple for samples of PMMA[TbSmL₁,ttpo] and in dark blue for samples PMMA[TbSmL₂,ttpo].

An emission map of PMMA[TbEuL₁tppo]1@SiO₂, which was measured over the temperature range from 5 to 50 °C, is presented in Figure 8a. The I_{543}/I_{614} intensity ratio of the integrated areas under the peaks for PMMA[TbEuL₁tppo]1@SiO₂ was calculated (Figure 8b), for the mentioned temperature range, over which the sample showed monotonic behavior. The data points could be well fitted by using Equation (2), yielding $\Delta E = 3143 \text{ cm}^{-1}$ ($R^2 = 0.9936$). The calculated energy difference can be well matched with the energy difference between the emitting level of Tb³⁺ ⁵D₄ (20500 cm⁻¹) and the emitting level of Eu³⁺ ⁵D₀ (17300 cm⁻¹). In Figure 8c, the relative sensitivity, S_r , calculated at different temperatures is presented. The maximal value of $S_r = 3.84 \% ^\circ\text{C}^{-1}$ obtained at 20 °C indicates that this sample shows very good thermometric behavior, as highlighted by a comparison with values reported in the literature (Table 3).

An emission map of PMMA[TbSmL₂tppo]3@SiO₂, measured over the temperature range from 5 to 50 °C, is presented in Figure 9a. The I_{543}/I_{643} intensity ratio of the integrated areas under the peaks for PMMA[TbSmL₂tppo]3@SiO₂ has been calculated (Figure 9b). The sample shows monotonic behavior over the indicated temperature range. The data points could be well fitted by using Equation (2), yielding $\Delta E = 2533 \text{ cm}^{-1}$ ($R^2 = 0.9987$). The calculated energy difference again matched well with the energy difference between the emitting level of Tb³⁺ ⁵D₄ (20500 cm⁻¹) and emitting level of Sm³⁺ ⁵G_{5/2} (17900 cm⁻¹). In Figure 9c, the relative sensitivity, S_r , calculated for the different temperatures is presented, showing a maximum value of $S_r = 3.27 \% ^\circ\text{C}^{-1}$ at 20 °C, which is among the best performing thermometers in water for this system (Table 3).

The results obtained for the samples herein show similar or higher sensitivity to that of the examples from the literature, except for one example,^[51] which was measured in the solid state. Our samples based on the Tb³⁺ – Eu³⁺ system are over 12 times more sensitive than that of samples based on the same system, and the samples based on the Tb³⁺ – Sm³⁺ system are up to 1% more sensitive than that of the most sensitive example presented to date.

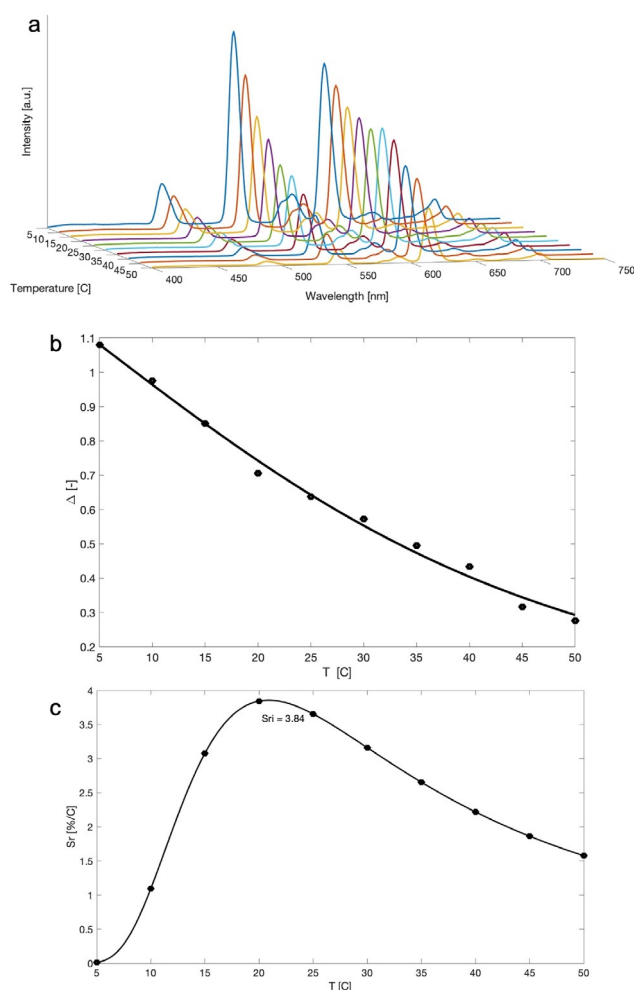


Figure 8. a) Emission map of PMMA[TbEuL₁tppo]1@SiO₂ NPs measured over the 5–50 °C range (step 5 °C). b) Plot representing the calibration curve for PMMA[TbEuL₁tppo]1@SiO₂. The points show the experimental Δ parameter and the solid line is the best fit of the experimental points by using Equation (2). c) Plot showing the relative sensitivity, S_r , values at different temperatures (5–50 °C); the solid line is intended as a guide to the eye.

Table 3. A comparison of the sensitivity of our thermometers with the sensitivity of other luminescent thermometers over the physiological temperature range. An overview of the materials, temperature range [°C], and maximal relative sensitivity value (S_m) is provided.

Material ^[a]	T range [°C]	S_m [% °C ⁻¹] ([°C])	Medium	Ref.
BPy-PMO@Tb,Sm(acac) ₃ -20_80	5–50	2.72 (5)	solution	[36]
ZJU-88J⊃perylene	20–80	1.28 (20)	solution	[47]
ZJU-28⊃DPASD-1	20–60	3.39 (60)	solution	[48]
[Tb(dipicCbz) ₃] ³⁻	25–79	3.40 (35)	solution	[49]
THA@EuNMOF@Fe/TA	20–60	0.6 (60)	tissue	[50]
Eu _{0.058} Tb _{0.942} BPT	20–80	7.22 (80)	solid state	[51]
Tb _{0.99} Eu _{0.01} (BDC) _{1.5} (H ₂ O) ₂	25–47	0.31 (45)	solution	[52]
PMMA[TbEuL ₁ tppo]1@SiO ₂	5–50	3.84 (20)	solution	this work
PMMA[TbEuL ₂ tppo]3@SiO ₂	5–50	3.05 (20)	solution	this work
PMMA[TbSmL ₁ tppo]1@SiO ₂	5–50	2.93 (15)	solution	this work
PMMA[TbSmL ₂ tppo]3@SiO ₂	5–50	3.27 (20)	solution	this work

[a] dipicCbz = 4-(9H-carbazol-9-yl)pyridine-2,6-dicarboxylate, NMOF = nanoscale metal-organic framework, TA = tannic acid, H₃BPT = biphenyl-3,4',5-tricarboxylate acid, BDC = 1-4-benzendicarboxylate.

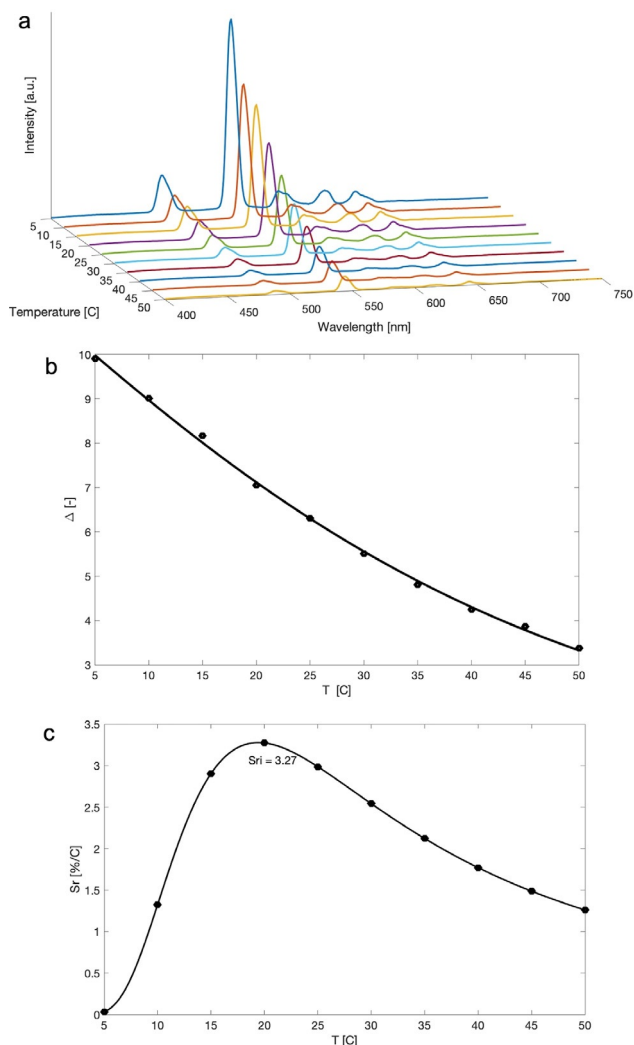


Figure 9. a) Emission map of PMMA[TbSmL₂tpo]1@SiO₂ NPs measured over the 5–50 °C range (step 5 °C). b) Plot representing the calibration curve for PMMA[TbSmL₂tpo]1@SiO₂. The points show the experimental ΔF parameter and the solid line is the best fit of the experimental points by using Equation (2). c) Plot showing the relative sensitivity, S_r , values at different temperatures (5–50 °C); the solid line is intended as a guide to the eye.

The temperature uncertainty, δT , calculated for the above-mentioned samples remains below 1 K over the whole studied temperature range, confirming the excellent behavior of these thermometers (Figure 10). For the PMMA[TbEuL₁tpo]1@SiO₂ NPs (Figure 10a), the temperature uncertainty, δT , is more consistent, and it is in the range from 0.015 to 0.03 °C, whereas for the PMMA[TbSmL₂tpo]3@SiO₂ NPs (Figure 10b) δT is in the range from 0.1 to 0.24 °C. The difference in δT comes from the intensity of the emission peaks, which is used for ratiometric temperature sensing in these two systems. In the physiological temperature range, the emission intensity of the Sm³⁺ peak at 643 nm (⁵G_{5/2} → ⁶H_{9/2}) is significantly lower than that of the emission intensity of the Eu³⁺ peak at 614 nm (⁵D₀ → ⁷F₂), which leads to a possibly higher uncertainty due to an increase of the background noise during temperature readout for thermometers based on the Tb³⁺ – Sm³⁺ system compared with those based on the Tb³⁺ – Eu³⁺ system.

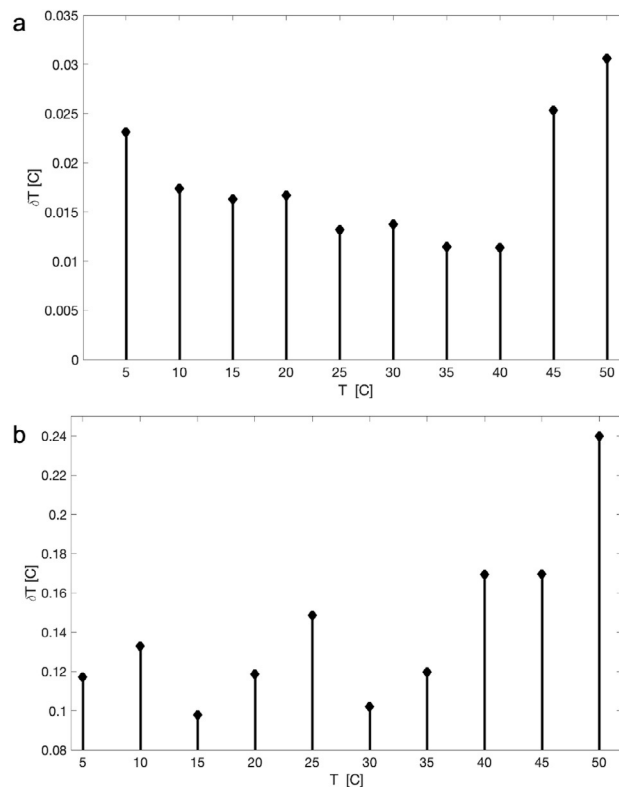


Figure 10. Calculated temperature uncertainty, δT , for PMMA[TbEuL₁tpo]1@SiO₂ NPs (a) and PMMA[TbSmL₂tpo]3@SiO₂ NPs (b).

Toxicity tests

To fully assess the potential use of PMMA-coated SiO₂ NPs for biological applications, cytotoxicity tests were conducted on living cells. Normal human dermal fibroblastic (NHDF) cells were used for these experiments. The results of the viability test demonstrated that the PMMA[TbEuL₁tpo]1@SiO₂ and PMMA[TbSmL₂tpo]3@SiO₂ NPs samples are nontoxic (Figure 11). At rather high concentrations of 1, 0.5, and 0.1 mg per well, the particles have shown toxicity towards fibroblastic cells. Cell viability at these concentration ranges from 20 to 40%, which shows a toxic effect. Disruption of cell adhesion and morphology was indicated by round cell morphology at concentrations of 1, 0.5, and 0.1 mg per well (Figure 11b). At a concentration of 0.05 mg per well, cells start to attach better, a higher number of cells have a spindle-shaped morphology, which is inherent in NHDF cells. ANOVA results showed a strong difference between the control at concentrations of 1, 0.5, and 0.1 mg per well. Most likely, at these concentrations, NPs tend to conglomerate, which can lead to mechanical pressure on the cells and stop cell adhesion. At concentrations of 0.05 mg per well and lower, the cell viability is 75% or higher (Figure 11a), which is considered to be almost nontoxic.^[53]

Conclusion

Thin PMMA films and PMMA-coated SiO₂ NP thermometers doped with tppo derivatives of lanthanide β -diketonate complexes showed very good temperature-sensing properties over

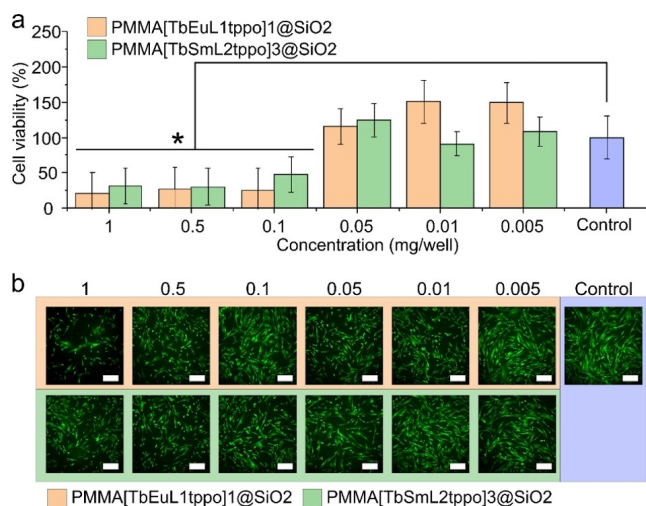


Figure 11. a) Cell viability after exposure to different concentrations of PMMA[TbEuL₁tppo]1@SiO₂ and PMMA[TbSmL₂tppo]3@SiO₂ NPs. An asterisk (*) indicates significant differences from the control cell group. Statistical analysis was performed by analysis of variance (ANOVA) followed by the Tukey test ($p < 0.05$). b) Fluorescence microscopy images of cells at different SiO₂-coated NP concentrations (cells are green). Scale bar: 250 μm .

the physiological temperature range. The thermometers were based on two ion-pair systems, Tb³⁺ – Eu³⁺ and Tb³⁺ – Sm³⁺, in which lanthanide ions were doped in the PMMA polymer in different ratios for a series of samples with L₁ and L₂ complexes. The results obtained for the PMMA films in both systems showed promising results for this temperature range, for which the Tb³⁺ – Eu³⁺ pair had S_r values in the range from 3.57 to 4.21 %K⁻¹, reaching the highest obtained value of $S_r = 4.21\% \text{K}^{-1}$ at 313 K for the PMMA[TbEuL₁tppo]1 sample. For the second system, the Tb³⁺ – Sm³⁺ pair, the S_r values were in the range from 2.93 to 3.64 %K⁻¹, with the highest value of $S_r = 3.64\% \text{K}^{-1}$ at 313 K found for the PMMA[TbSmL₂tppo]3 sample. The best performing samples, one from each series of PMMA films, were used to coat the SiO₂ NPs, and the results showed that the relative sensitivity were similar to those in the films, with only slightly lower S_r values. The value of $S_r = 3.84\% \text{K}^{-1}$ at 20 °C was retrieved for the PMMA-[TbEuL₁tppo]1@SiO₂ sample, whereas the PMMA[TbSmL₂tppo]3@SiO₂ sample had a value of $S_r = 3.27\% \text{K}^{-1}$ at 20 °C. The obtained results of relative sensitivity reported for PMMA films are among the highest values for the physiological temperature range in both the solid state and water, as coatings of SiO₂ NPs. The promising results of the toxicity tests give an opportunity for future work with in vitro and in vivo measurements of temperature with PMMA-coated SiO₂ NPs.

Experimental Section

Preparation of PMMA films doped with [Ln₁(L₁₍₂₎)₃(tppo)₂] and [Ln₂(L₁₍₂₎)₃(tppo)₂] complexes (Ln₁ = Tb³⁺; Ln₂ = Eu³⁺, Sm³⁺)

The PMMA films were prepared as follows: PMMA (100 mg) was weighed and placed in a 25 mL vial. It was dissolved in chloroform (10 mL) and stirred at room temperature for 15 min. Solutions of complexes [Ln₁(L₁₍₂₎)₃(tppo)₂] and [Ln₂(L₁₍₂₎)₃(tppo)₂] (Ln₁ = Tb³⁺ and Ln₂ = Eu³⁺ or Sm³⁺) were prepared by dissolving different ratios of Ln₁ and Ln₂ complexes in chloroform (3 mL) with total concentrations of complexes in the range of 1.67×10^{-3} to $1.67 \times 10^{-2} \text{mol L}^{-1}$, depending of the ratio used for lanthanide complexes, to obtain different intensity ratios of emission peaks of Ln₁ and Ln₂. The solutions of lanthanide complexes were added dropwise to the solution of PMMA and left to stir for 2 h. After this time, the solution was transferred to a Petri dish and a heating plate at 30 °C was used to evaporate chloroform and form clear films.

Preparation of SiO₂ NPs coated with PMMA[Ln₁Ln₂L₁₍₂₎tppo] films

The silica NPs were synthesized by a procedure previously established in our group.^[54] The coating of the SiO₂ NPs was done as follows: PMMA[Ln₁Ln₂L₁₍₂₎tppo] (50 mg) was dissolved in chloroform (5 mL) and an excess of PMMA (40 mg) was added, and the solution was left to stir for 30 min at room temperature. At the same time, SiO₂ NPs (70 mg) were dispersed in chloroform (3 mL), and after 30 min of stirring the SiO₂ NP suspension was added to the solution of PMMA[Ln₁Ln₂L₁₍₂₎tppo] and left to stir for 2 h. Afterwards, the suspension was transferred to a 15 mL centrifuge tube and centrifuged for 5 min at 5000 rpm to separate the SiO₂ NPs from the rest of the solution of PMMA. The solution of PMMA was decanted and the PMMA[Ln₁Ln₂L₁₍₂₎tppo]@SiO₂ NPs were left to dry in open air for 1 d. The next day, the NPs were washed once with a mixture of methanol/water (1/1, v/v) to remove residual unreacted PMMA. After washing and decanting of the rinsing solvent, the NPs were left to dry in open air for 1 d.

Details of the characterization of the PMMA films doped with [Ln₁Ln₂(L₁₍₂₎)₃(tppo)₂] and the SiO₂ NPs coated with PMMA [Ln₁Ln₂L₁₍₂₎tppo] films can be found in the Supporting Information. Deposition Numbers 1964128, 1964129, 1964130, 1964131, and 1964132 contain the supplementary crystallographic data for this paper. These data are provided free of charge by the joint Cambridge Crystallographic Data Centre and Fachinformationszentrum Karlsruhe Access Structures service www.ccdc.cam.ac.uk/structures.

Acknowledgements

D.M. and R.V.D. acknowledge the Ghent University Special Research Fund (BOF) for Ph.D. grants (BOF15/24J/049). D.M. acknowledges KU Leuven Postdoctoral Mandate Internal Funds (PDM) for a postdoctoral fellowship (PDM/20/092). A.M.K. acknowledges Ghent University for funding. F.A. acknowledges the FWO (Research Foundation Flanders) and the European Union's Horizon 2020 program for a [Pegasus]² Marie Skłodowska-Curie fellowship "Nanocomposite materials for highly efficient sensitized lanthanide emission". K.V.H. thanks the Hercules Foundation (project AUGÉ/11/029 "3D-SPACE: 3D Structural Platform Aiming for Chemical Excellence") and the Special

Research Fund (BOF)—UGent (project 01N03217) for funding. A.G.S. acknowledges the Special Research Fund (BOF)—UGent (projects 01I03618, BOF14/IOP/003) and FWO (G043219) for support.

Conflict of interest

The authors declare no conflict of interest.

Keywords: organic–inorganic hybrid composites · lanthanides · luminescent thermometry · nanoparticles · thin films

- [1] P. R. N. Childs, J. R. Greenwood, C. A. Long, *Rev. Sci. Instrum.* **2000**, *71*, 2959–2978.
- [2] C. D. S. Brites, S. Balabhadra, L. D. Carlos, *Adv. Opt. Mater.* **2019**, *7*, 1801239.
- [3] K. M. McCabe, M. Hernandez, *Periatr. Res.* **2010**, *67*, 469–475.
- [4] D. Jaque, L. M. Maestro, B. del Rosal, P. Haro-Gonzalez, A. Bemayas, J. L. Plaza, E. M. Rodríguez, J. G. Solé, *Nanoscale* **2014**, *6*, 9494–9530.
- [5] C. D. S. Brites, P. P. Lima, N. J. O. Silva, A. Millán, V. S. Amaral, F. Palacio, L. D. Carlos, *New J. Chem.* **2011**, *35*, 1177–1183.
- [6] S. Uchiyama, C. Gota, T. Tsuji, N. Inada, *Chem. Commun.* **2017**, *53*, 10976–10992.
- [7] D. Jaque, F. Ventrone, *Nanoscale* **2012**, *4*, 4301–4326.
- [8] X. D. Wang, O. S. Wolfbeis, R. J. Meier, *Chem. Soc. Rev.* **2013**, *42*, 7834–7869.
- [9] A. G. Skirtach, A. Muñoz Javier, O. Kreft, K. Köhler, A. Piera Alberola, H. Möhrowald, W. J. Parak, G. B. Sukhorukov, *Angew. Chem. Int. Ed.* **2006**, *45*, 4612–4617; *Angew. Chem.* **2006**, *118*, 4728–4733.
- [10] J. Zhong, D. Chen, Y. Peng, Y. Lu, X. Chen, X. Li, Z. Ji, *J. Alloys Compd.* **2018**, *763*, 34–48.
- [11] A. M. Stark, S. Way, *Cancer* **1974**, *33*, 1664–1670.
- [12] A. M. Stark, S. Way, *Cancer* **1974**, *33*, 1671–1679.
- [13] J. Rocha, C. D. S. Brites, L. D. Carlos, *Chem. Eur. J.* **2016**, *22*, 14782.
- [14] S. Uchiyama, C. Gota, *Rev. Anal. Chem.* **2017**, *36*, 20160021.
- [15] Y. Wu, J. Liu, J. Ma, Y. Liu, Y. Wang, D. Wu, *ACS Appl. Mater. Interfaces* **2016**, *8*, 14396–14405.
- [16] A. Soleilhac, M. Girod, P. Dugour, B. Burdin, J. Parvole, P.-Y. Dugas, F. Beyard, E. Lacôte, E. Bourget-Lami, R. Antoine, *Langmuir* **2016**, *32*, 4052–4058.
- [17] L. Wei, Y. Ma, X. Shi, Y. Wang, X. Su, C. Yu, S. Xiang, L. Xiao, B. Chen, *J. Mater. Chem. B* **2017**, *5*, 3383–3390.
- [18] A. G. Skirtach, C. Dejugant, D. Braun, A. S. Susha, A. L. Rogach, W. J. Parak, H. Möhrowald, G. B. Sukhorukov, *Nano Lett.* **2005**, *5*, 1371–1377.
- [19] J.-C. G. Bünzli, *Coord. Chem. Rev.* **2015**, *293*, 19–47.
- [20] L. D. Carlos, R. A. S. Ferreira, V. de Zea Bermudez, S. J. L. Ribeiro, *Adv. Mater.* **2009**, *21*, 509–534.
- [21] A. de Bettencourt-Dias, *Luminescence of Lanthanide Ions in Coordination Compounds and Nanomaterials*, Wiley, Hoboken, **2014**.
- [22] J.-C. G. Bünzli, *Handbook on the Physics and Chemistry of Rare Earths, Vol. 50* (Eds.: J.-C. G. Bünzli, K. V. Pecharsky), Elsevier B. V., Amsterdam, **2016**, pp. 141–175.
- [23] C. D. S. Brites, A. Millán, L. D. Carlos, *Handbook on the Physics and Chemistry of Rare Earths, Vol. 49* (Eds.: J.-C. G. Bünzli, K. V. Pecharsky), Elsevier B. V., Amsterdam, **2016**, pp. 339–427.
- [24] J.-C. G. Bünzli, C. Piquet, *Chem. Soc. Rev.* **2005**, *34*, 1048–1077.
- [25] L. Armelao, S. Quici, F. Barigellati, G. Accorsi, G. Bottaro, M. Cavazzini, E. Tondello, *Coord. Chem. Rev.* **2010**, *254*, 487–505.
- [26] K. Binnemans, *Handbook on the Physics and Chemistry of Rare Earths, Vol. 35* (Eds.: K. A. Gschneider, Jr, J.-C. G. Bünzli, V. K. Pecharsky), Elsevier B. V., Amsterdam, **2005**, pp. 107–272.
- [27] K. Binnemans, *Chem. Rev.* **2009**, *109*, 4283–4373.
- [28] D. Mara, F. Artizzu, P. F. Smet, A. M. Kaczmarek, K. Van Hecke, R. Van Deun, *Chem. Eur. J.* **2019**, *25*, 15944–15956.
- [29] J. Kai, M. C. F. C. Felinto, L. A. O. Nunes, O. L. Malta, H. F. Brito, *J. Mater. Chem.* **2011**, *21*, 3796–3802.
- [30] D. Mara, F. Artizzu, B. Laforce, L. Vincze, K. Van Hecke, R. Van Deun, A. M. Kaczmarek, *J. Lumin.* **2019**, *213*, 343–355.
- [31] Y. Cui, F. Zhu, B. Chen, G. Qian, *Chem. Commun.* **2015**, *51*, 7420–7431.
- [32] Y. Pan, H.-Q. Su, E.-L. Zhou, H.-Z. Yin, K.-Z. Shao, Z.-M. Su, *Dalton Trans.* **2019**, *48*, 3723–3729.
- [33] C. D. S. Brites, P. P. Lima, L. D. Carlos, *J. Lumin.* **2016**, *169*, 497–502.
- [34] J. K. Zareba, M. Nyk, J. Janczak, M. Samoć, *ACS Appl. Mater. Interfaces* **2019**, *11*, 10435–10441.
- [35] A. M. Kaczmarek, R. Van Deun, P. Van Der Voort, *J. Mater. Chem. C* **2019**, *7*, 422–4229.
- [36] A. M. Kaczmarek, Y. Maegawa, A. Abalymov, A. G. Skirtach, S. Inagaki, P. Van Der Voort, *ACS Appl. Mater. Interfaces* **2020**, *12*, 13540–13550.
- [37] M. Dramićanin, *Luminescence Thermometry, Methods, Materials and Applications*, Woodhead, Oxford, **2018**.
- [38] A. M. Kaczmarek, R. Van Deun, M. K. Kaczmarek, *Sensors Actuators B Chem.* **2018**, *273*, 696–702.
- [39] Y. Yang, H. Huang, Y. Wang, F. Qui, Y. Feng, X. Song, X. Tang, G. Zhang, W. Liu, *Dalton Trans.* **2018**, *47*, 13384–13390.
- [40] T. Chuusaard, A. Ngamajarujana, S. Surinwong, T. Konnd, S. Bureekaew, A. Rujiwatra, *Inorg. Chem.* **2018**, *57*, 2620–2630.
- [41] J.-F. Feng, S.-Y. Gao, T.-F. Liu, J. Sai, R. Cao, *ACS Appl. Mater. Interfaces* **2018**, *10*, 6014–6023.
- [42] F. Ruan, D. Deng, M. Wu, B. Chen, R. Lei, S. Xu, *J. Lumin.* **2019**, *213*, 117–126.
- [43] P. Farger, C. Leuvere, M. Gallart, P. Gilliot, G. Rogez, J. Rocha, D. Ananias, P. Rabu, E. Delahaye, *Beilstein J. Nanotechnol.* **2018**, *9*, 2775–2787.
- [44] X. Zhou, H. Wang, S. Jiang, G. Xiang, X. Tang, X. Luo, Z. Li, X. Zhou, *Inorg. Chem.* **2019**, *58*, 3780–3788.
- [45] D. Zhao, X. Rao, J. Yu, Y. Cui, Y. Yang, G. Qian, *Inorg. Chem.* **2015**, *54*, 11193–11199.
- [46] Ch. J. Salas-Juárez, R. E. Navarro, A. Pérez-Rodríguez, U. Orozco-Valencia, R. Aceves, *Sensors Actuators A* **2020**, *315*, 112293.
- [47] Y. Cui, R. Song, J. Yu, M. Liu, Z. Wang, C. Wu, Y. Yang, Z. Wang, B. Chen, G. Qian, *Adv. Mater.* **2015**, *27*, 1420–1425.
- [48] Y. Wan, T. Xia, Y. Cui, Y. Yang, G. Qian, *ChemPlusChem* **2017**, *82*, 1320–1325.
- [49] J. H. S. K. Monteiro, F. A. Sigoli, A. de Bettencourt-Dias, *Can. J. Chem.* **2018**, *96*, 859–864.
- [50] H. Yan, H. Ni, J. Jia, C. Shan, T. Zhang, Y. Gong, X. Li, J. Cao, W. Wu, W. Liu, T. Tang, *Anal. Chem.* **2019**, *91*, 5225–5234.
- [51] L. Zhang, Y. Xie, T. Xia, Y. Cui, Y. Yang, G. Qian, *J. Rare Earth.* **2018**, *36*, 561–566.
- [52] A. Cadiou, C. D. S. Brites, P. M. F. J. Costa, R. A. S. Ferreira, J. Rocha, L. D. Carlos, *ACS Nano* **2013**, *7*, 7213–7218.
- [53] ISO 10993–5:2009, *Biological Evaluation of Medical Devices: Part 5: Test for in vitro Cytotoxicity*, Canadian Standards Association, **2007**, pp. 1–11.
- [54] F. Artizzu, D. Loche, D. Mara, D. Manu, I. Malfatti, A. Serpe, R. Van Deun, M. F. Casula, *J. Mater. Chem. C* **2018**, *6*, 7479–7486.

Manuscript received: November 13, 2020

Revised manuscript received: January 20, 2021

Accepted manuscript online: January 21, 2021

Version of record online: March 11, 2021